European Journal of Medicinal Chemistry 100 (2015) 106–118

Contents lists available at ScienceDirect

European Journal of Medicinal Chemistry

journal homepage: http://www.elsevier.com/locate/ejmech

Research paper

1,5-Diarylpyrazole and vanillin hybrids: Synthesis, biological activity and DFT studies

Eduardo Hernández-Vázquez [a, *], Romina Castañeda-Arriaga [b], Juan José Ramírez-Espinosa [d], Omar Noel Medina-Campos [c], Francisco Hernández-Luis [a], José Pedraza Chaverri [c], Samuel Estrada-Soto [d]

[a] Facultad de Química, Departamento de Farmacia, Universidad Nacional Autónoma de México, México, DF 04510, Mexico
[b] Facultad de Química, Departamento de Física y Química Teórica, Universidad Nacional Autónoma de México, México, DF 04510, Mexico
[c] Facultad de Química, Departamento de Biología, Universidad Nacional Autónoma de México, México, DF 04510, Mexico
[d] Facultad de Farmacia, Universidad Autónoma del Estado de Morelos, Cuernavaca, Morelos 62209, Mexico

ARTICLE INFO

Article history:
Received 23 February 2015
Received in revised form
2 June 2015
Accepted 3 June 2015
Available online 5 June 2015

Keywords:
Diarylpyrazole hybrids
Vanillin
Antioxidant capacity
DFT calculations

ABSTRACT

Herein, we report the design and synthesis of 13 diarylpyrazole hybrids with vanillin constructed as dual compounds against oxidative stress and diabetes. Compounds were tested in two different antioxidant assays. It was found that all compounds showed an important antioxidant activity in both DPPH and ORAC models and the activity was even more remarkable than vanillin. In addition, the hypoglycemic effect of compounds **1**, **2**, **4** and **12** was evaluated. Interestingly, compound **1** had the most potent hypoglycemic effect with a glycemia reduction of 71%, which was higher than rimonabant. Finally, a DFT study to propose a reasonable antioxidant mechanism is detailed. Both thermodynamic and kinetic studies indicated that the most feasible mechanism consists in the HAT abstraction of the phenolic hydrogen due to the formation of an stable transition state through the most rapid and exergonic path, while the SPLET mechanism is the most significant at higher pH values.

1. Introduction

Oxidative stress is defined as a redox imbalance generated by the overproduction of highly reactive species (oxygen, ROS; nitrogen, RNS), the deficiency of the antioxidant system (small molecules, proteins and enzymes) or both [1]. Several chronic diseases have been proposed to be either caused or enhanced by oxidative stress, such as obesity, cancer, aging, inflammation, neurodegenerative disorders, hypertension, and cardiovascular diseases [2]. Furthermore, the participation of oxidative stress in the development and progression of diabetes and its complications is widely accepted [3,4]. ROS formation is a direct consequence of hyperglycemia (Fig. 1) [5], and several mechanisms contribute to its formation. In mitochondria, high levels of glucose enhance superoxide production, which eventually activates the nuclear enzyme poly (ADP-ribose) polymerase (PARP) and inhibits glyceraldehyde-3-phosphate dehydrogenase (GAPDH) [6,7]. As a result of that, other glucose catabolic pathways become activated, such as hexosamine and polyol (sorbitol-aldose reductive pathway) metabolic cascades. Furthermore, hexosamine pathway is a well-known source of endogenous radicals, while the activation of polyol route depletes nicotinamide adenine dinucleotide phosphate (NADPH), a necessary cofactor to regenerate oxidized glutathione [7,8]. Likewise, other mechanisms related to diabetic complications are activated, like protein kinase C (PKC) and advanced glycation end products (AGE) [9,10], which eventually lead to ROS production. Besides the latter, transition-metal dependent autooxidation and nonenzymatic glycation of glucose with amino groups of proteins or nucleic acids, contribute to oxidative stress in hyperglycemia [11]. As a result of the activation of all those mechanisms, oxidative stress participates in pathogenesis of diabetes due to their ability to directly oxidize and damage lipids, DNA and proteins. Some radicals can also act as signaling molecules to activate stress-sensitive pathways [nuclear factor kappa B (NF-κB), p38 mitogen-activated protein kinase (p38 MAPK), c-Jun N-terminal kinase (JNK)/stress-activated protein kinase (SAPK)] [5,12], which finally produce insulin resistance and β-cell damage [9,13,14]. For these reasons, antioxidants could be employed in diabetes treatment and

* Corresponding author.
E-mail address: eduardo.hervaz@gmail.com (E. Hernández-Vázquez).

http://dx.doi.org/10.1016/j.ejmech.2015.06.010
0223-5234/

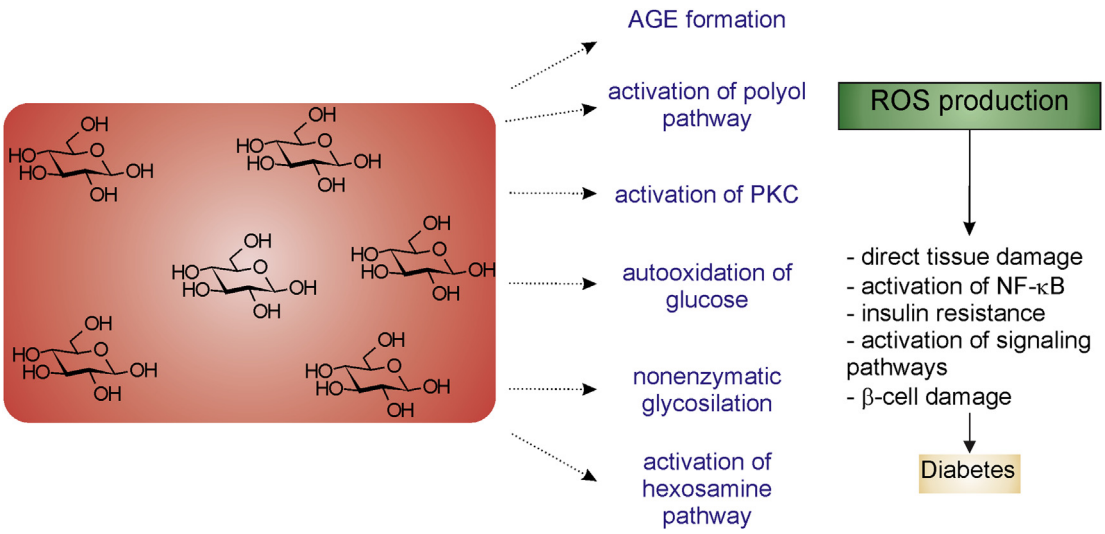

Fig. 1. Relationship between oxidative stress and diabetes.

also in the prevention of its complications. However, only a limited number of antioxidants are capable to reduce high blood glucose levels in diabetes such as melatonin, vitamins C and E (with β-carotene) and lipoic acid [15–17].

On the other hand, it is well documented the participation of cannabinoid receptor 1 (CB1) in metabolic control and food intake balance [18]. In particular, the antagonism of CB1 triggers signal pathways in peripheral organs (liver, adipose tissue and skeletal muscle) that regulate metabolic functions like the reduction of adipogenesis, hypoglycemia by glucose uptake, thermogenesis, enhancement of lipogenesis and adiponectin up-regulation [19–21]. In accordance to this, our group has reported a series of 1,5-diarylpyrazole with higher hypoglycemic activity than rimonabant, a selective CB1 antagonist [22]. However, several trials have shown that improving glycemic control does not necessarily reduce the collateral oxidative stress [23]. Therefore, the main objective of this work was the hybridization of 1,5-diarylpyrazole analogs and vanillin, with the purpose of generating a new class of compounds to offer an integral treatment to diabetes and metabolic syndrome (Fig. 2). The design considered the formation of a hydrazone in order to act as a bioisostere of guaiacol derivatives. The increase in conjugation of π-electrons would confer a higher degree of resonance structures of the phenoxy radical, which has been proposed to be the mechanism implicated in the antioxidant activity of these derivatives [24,25], and thus would enhance the protective effect against oxidative stress.

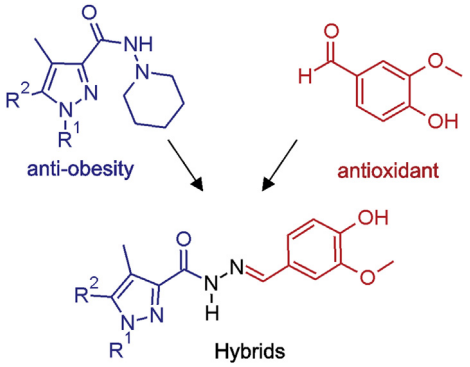

Fig. 2. Design of pyrazole-based hybrids.

2. Results and discussion

2.1. Chemistry

The synthetic pathway observed in Scheme 1 was followed for the synthesis of hybrids **1**–**13**. First, the 1,5-diaryl pyrazole-3-carboylic acids were constructed. To achieve these intermediaries, different substituted propiophenone derivatives were treated with lithium *bis*(trimethylsilyl)amide (LiHMDS) in methylcyclohexane, giving the corresponding lithium enolates. These enolates were left to react with diethyl oxalate to obtain the expected ethyl 4-aryl-3-methyl-2,4-dioxobutanoate (compounds **19**–**31**), with yields ranging from 60% to 97% (Scheme 1). The cyclocondensation of previously obtained phenylhydrazines and the unpurified tricarbonylic compounds in a sulfuric acid/ethanol solution produced the ethyl pyrazole-3-carboxylates. The esters were converted to the corresponding carboxylic acids by treatment with potassium hydroxide at 50 °C, resulting in an overall yield ranging from 50 to 87%.

After that, we focused on the synthesis of final products. Two routes were considered to achieve compounds **1**–**13**. In a first attempt, the vanillin hydrazone was proposed as an intermediary; however, the dimerization of the aldehyde was the major product when treated vanillin with hydrazine hydrochloride; similar result was observed when the *N*-Boc carbazate was deprotected. This problem was solved by changing the order of the hydrazone formation. As seen in Scheme 1, the pyrazole-3-carboxylic acids were converted to the corresponding acyl chlorides by refluxing them with thionyl chloride in toluene and later were stirred with *tert*-butyl carbazate to obtain the desired carbohydrazides in good yields. Without purification, Boc group was cleavage by treatment with trifluoroacetic acid (TFA) and subsequently condensed with vanillin to afford hydrazones **1**–**13**. Table 1 resumes the physicochemical properties of compounds, which were obtained as solids with a narrow melting point.

During the condensation of vanillin with 1,5-diarylpyrazole-3-carbohydrazides, two possible configurations are expected: the *Z* and the *E* hydrazones (Fig. 3); despite this possibility, only one compound was observed. In the case of the *E* isomer, H^a (hydrogen bonded to the nitrogen) can interact with the imine hydrogen H^b and with the hydrogen at *ortho* position of phenol ring (H^c and $H^{c'}$), while the *Z* isomer can only couple with $H^c/H^{c'}$. In order to verify the

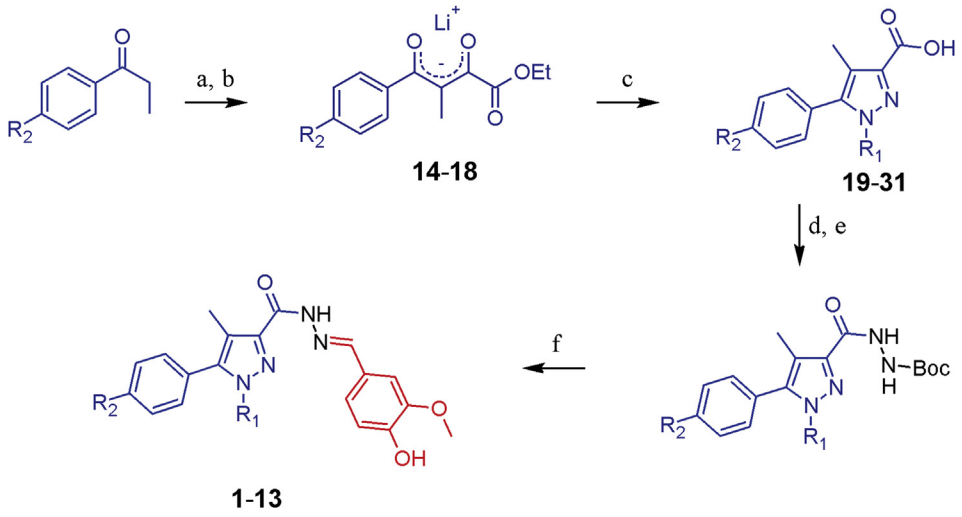

Scheme 1. Synthesis of hybrids **1**–**13**. Reagents and conditions: a) LiHMDS, MCH, 3 h, r.t. b) diethyl oxalate, r.t. c) corresponding arylhydrazine, H_2SO_4, EtOH, 80 °C, ca. 8 h then KOH, EtOH, 50 °C, 12. d) $SOCl_2$, PhMe, 110 °C, ca. 2.5 h e) *t*-butyl carbazate, DIPEA, $CHCl_3$, 0 °C to r. t., 3 h f) TFA, then vanillin, $AcOH_{cat}$, $CHCl_3$, r.t.

Table 1
Physicochemical data of compounds **1**–**13**.

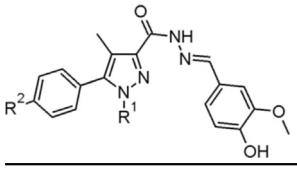

Compound	R^1	R^2	Melting point (°C)	Unoptimized yield (%)
1	2,4-Dichlorophenyl	Cl	256–258	68
2	2,4-Dichlorophenyl	H	239–241	69
3	Phenyl	H	291–292	62
4	3,4-Dichlorophenyl	Cl	224	60
5	3-Chloro-4-fluorophenyl	Cl	210–212	62
6	7-Chloroquinolin-4-yl	Cl	272–273	59
7	4-(Trifluoromethyl)phenyl	Cl	184–185	51
8	2,4-Difluorophenyl	F	241–242	57
9	3-Chloro-4-fluorophenyl	F	206	84
10	7-Chloroquinolin-4-yl	F	289–291	55
11	4-(Trifluoromethyl)phenyl	Br	289–290	78
12	2,4-Dichlorophenyl	CF_3	250–251	76
13	2,4-Difluorophenyl	CF_3	245–246	87

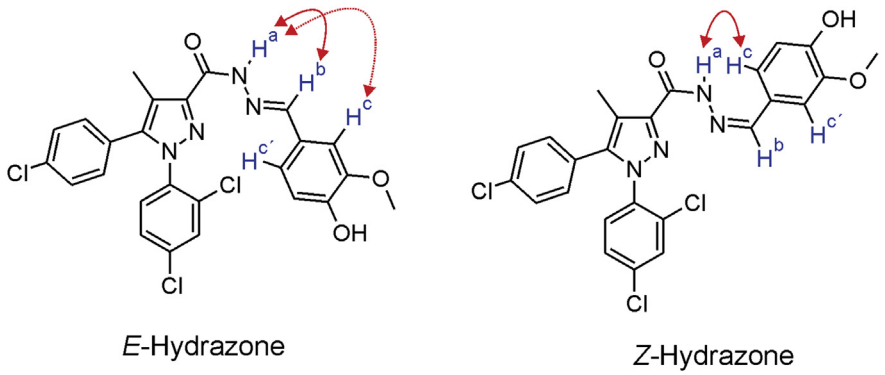

Fig. 3. Possible interactions throughout space in *E* and *Z* isomers of hybrids. Compound **1** is shown in the figure.

configuration of the series, the nuclear Overhauser effect spectroscopy (NOESY) spectrum of compound **2** was analyzed. Fig. 4 shows an expansion from 8 to 12 ppm of the spectrum of **2**. In this region, three signals can be observed: those corresponding to the hydrogen of the hydrazone (H^a, 11.6 ppm), the imine (H^b, 8.4 ppm) and the phenol (H^d, 9.5 ppm), respectively. As discussed

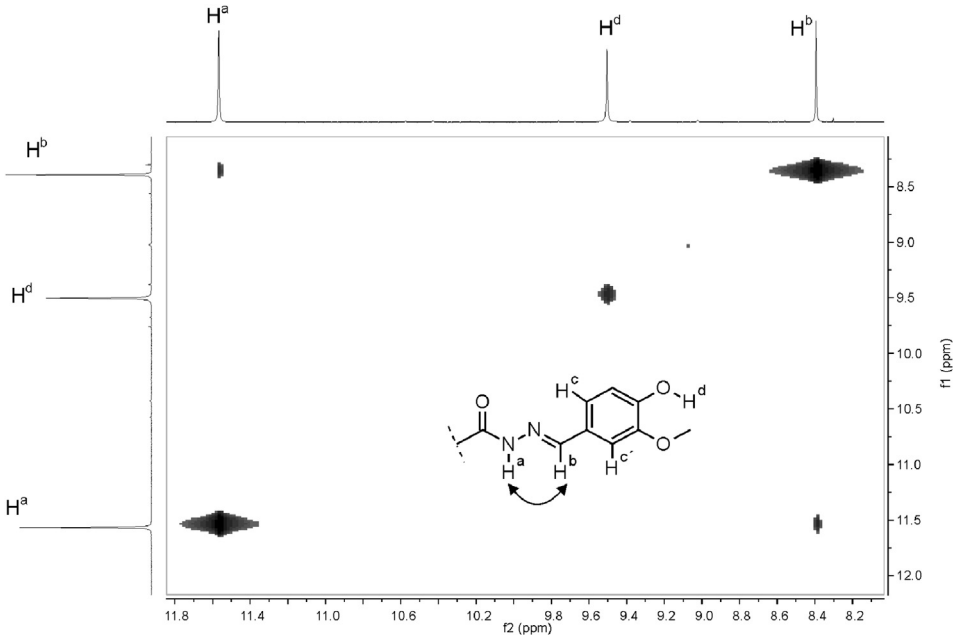

Fig. 4. NOESY spectrum of **2** (extension from 11.8 to 8.2 ppm). A correlation between H^a and H^b is clearly visible.

above, only the *E* isomer shows a correlation throughout space between the hydrazine and imine hydrogens (H^a and H^b, respectively), and this interaction is present in the NOESY spectrum of **2**. This interaction is due to the proximity of both atoms, which does not occur in the *Z* isomer. Additionally, a density functional theory (DFT) minimization with B3LYP 6-31G+ in a PCM solvation model was performed to further calculate the most stable isomer. Two compounds were submitted to this calculation (**2** and **13**), and in both cases, the *E* isomer was the most stable (Fig. 5). By analyzing the optimized geometry of the isomers, it can be clearly notice that the distance between H^a and H^b in *E* hydrazone is close enough to generate a correlation in NOESY spectrum. In summary, NOESY

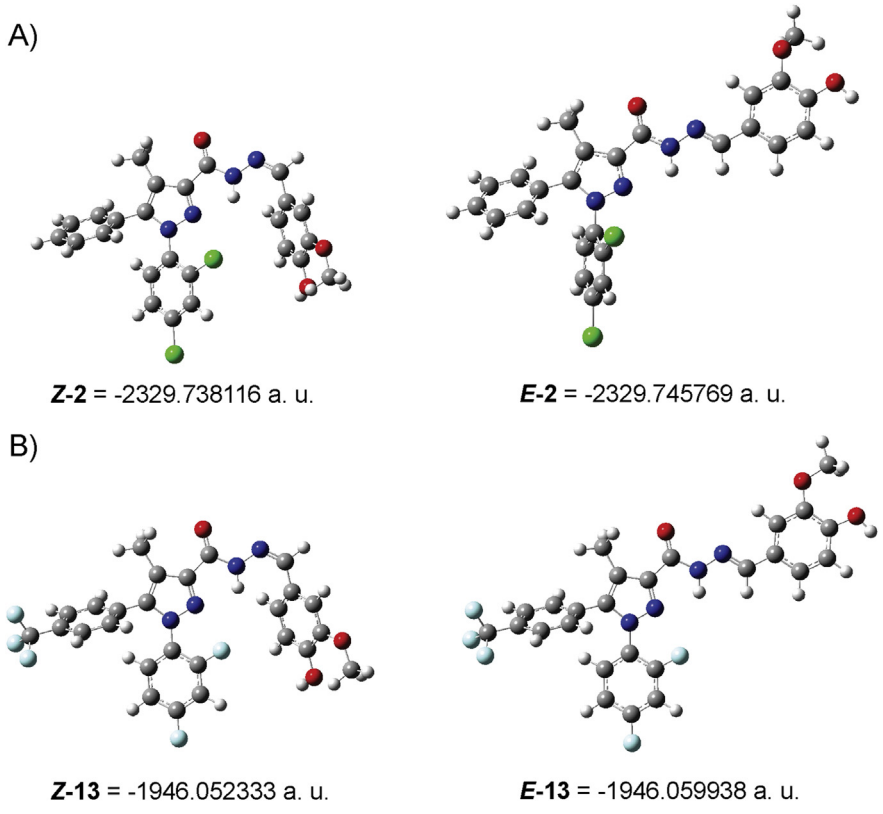

Fig. 5. DFT optimization of compounds **2** and **13**. A) Compound **2**. B) Compound **13**. In both cases, the *E* isomer is the most stable.

spectra and DFT calculations confirmed that *E* hydrazone is the geometry observed in the series.

2.2. Biology

2.2.1. In vitro antioxidant capacity

The design of compounds included an antioxidant portion, thus we decided to evaluate their radical scavenging capability. Several assays, such as trolox-equivalent antioxidant activity (TEAC), oxygen radical absorbance capacity (ORAC) assays as well as 2,2-diphenylpicrylhydrazyl (DPPH) scavenging, are commonly used to study the radical-scavenging ability of phenolic compounds [26,27], and provide a relative measure of antioxidant activity [28]. As a preliminary study, the DPPH-scavenging capacity was evaluated. DPPH is a stable radical which has been used to test the antioxidant capacity of foods and other compounds [29]. The EC_{50} of hybrids **1**–**13** is shown in Table 2. As it can be seen, all compounds had a DPPH-scavenging effect under 7 mM and compound **7** was the most active (EC_{50} = 2.34 mM). However, no significant differences between compounds were found and all compounds were less active than ascorbic acid. In order to corroborate if the antioxidant activity is directly related to the presence of vanillin moiety, the pirazole-3-carboxylic acid **19** was tested. As expected, this compound did not show an important DPPH scavenging activity (maximum scavenging of 17%), thus the antioxidant activity may be explained by the phenolic hydrazone. In addition, vanillin and vanillic acid were evaluated and, surprisingly, compounds **1**–**13** had a better DPPH scavenging capacity than those guaiacol derivatives. These findings suggest that the hybridization of vanillin with 1,5-diarylpyrazole derivatives not only maintained the antioxidant properties of this phenolic compound but also indicated an increase of activity due to the conjugation of both scaffolds.

Although interesting results were found with the DPPH-scavenging assay, this radical has no biological importance because it is not endogenous. For this reason, the ORAC assay was carried out since this technique can evaluate the ability of compounds to scavenge peroxyl radical ($ROO^{\bullet}$), a reactive oxygen specie with biological and clinical relevance [30]. ORAC method determines the ability of antioxidants to protect the oxidative damage in fluorescein caused by a source of peroxyl radicals through the measurement of the decrease in its fluorescence. Hybrids tested (Table 2) had an antioxidant capacity ranging from 401 to 1076 trolox equivalents and compound **2** was the most active. Unlike DPPH results, vanillic acid showed a better antioxidant capacity, being two-fold more active than **2**. This result clearly indicates that there is no correlation between the two methods employed, although both assays are considered hydrogen atom transfer (HAT) methodologies. Additionally, no structure-activity relationships can be generated because the antioxidant effect is due to the guaiacol moiety and the substitutions of phenyl ring slightly interferes in the global effect. Both DPPH and ORAC assays demonstrated the antioxidant properties of hybrids **1**–**13** and therefore can be considered as new antioxidant compounds. However, further scavenging studies comprising other ROS as well as *in vivo* models are required and the publication of these results is forthcoming.

Table 2
EC_{50} of DPPH-scavenging and trolox equivalents in ORAC for hybrids **1**–**13**.

Compound	DPPH scavenging (EC50)		ORAC
	(Mg/ml)	(mM)	Trolox equivalents/g
1	1.88	3.55	634 ± 83
2	1.48	2.99	1076 ± 224
3	1.05	2.46	611 ± 52
4	1.38	2.60	432 ± 32
5	1.83	3.56	882 ± 63
6	2.51	4.59	ND
7	1.24	2.34	867 ± 71
8	1.7	3.54	891 ± 45
9	3.44	6.92	525 ± 41
10	3.42	6.45	ND
11	1.67	2.91	ND
12	2.39	4.24	401 ± 42
13	1.54	2.90	993 ± 172
Vanillic acid	11.06	65.83	2979 ± 262
Vanillin	[a]	[a]	ND
19	[b]	[b]	ND
Ascorbic acid	0.366 ± 0.048	2.07 ± 0.034	ND

ND: not determined.
[a] Maximum scavenging of 7% at 20 g/mL (75% at 1 g/mL).
[b] Maximum scavenging of 17% at 20 mg/mL.

2.2.2. In vivo hypoglycemic evaluation

We have previously demonstrated that 1,5-diarylpyrazole derivatives having electron-withdrawing groups show a remarkable *in vivo* glucose reduction in diabetic rats [22], and in consequence, hybrids **1**–**13** could exhibit this effect. To further corroborate this statement, an *in vivo* diabetes mellitus type II (DMTII) test in previously induced diabetic rats was performed. Due to the poor solubility of compounds in water, we employed Tween 80 as vehicle. Furthermore, glibenclamide was taken as reference drug while vehicle was considered as control. The compounds tested showed a significant glycemia reduction with respect to the control (Table 3). Fig. 6 shows the glycemia reduction over the time of evaluation (7 h). The most prominent effect was evident at 7 h after administration of analogues, in which compounds **1**, **2**, **4**, and **12** showed a plasma glucose reduction of 71, 32, 39 and 41%, respectively. Compounds **4** and **12** had a similar response to that observed with the administration of glibenclamide and, as it can be deduced from Fig. 6, the effect would continue after 7 h. Even though this pharmacologic effect is significant, compound **1** had the best antidiabetic results, with an extraordinarily reduction of 71% at 7 h. It is remarkable that compound **2**, which 1,5-diarylpyrazole moiety lacks of CB1 affinity [31], also displayed an important glycemia reduction. Two assertions can be concluded from these data. First, the hybrids showed an *in vivo* antidiabetic activity and thus, the hybridization with vanillin did not eliminate the biological activity of rimonabant derivatives but conserved the antioxidant capacity. As result of that, it was confirmed that compounds **1**–**13** act as hybrids, in which two components of diabetes were covered: oxidative stress and hyperglycemia. Second, the hypoglycemic activity of rimonabant was increased. In previously published works, its percentage of glucose reduction in the same model was about 31% at 7 h [22]. Nonetheless, when rimonabant hybridizes with vanillin hydrazone, the effect increases to 71%. The depletion could be attributed to the antioxidant capacity, which could reduce the oxidative stress that is involved in the development and progression of diabetes. Moreover, an increase in peripheral CB1 receptor affinity is not discarded. This is a vital point in the design of CB1 antagonist/inverse agonist for the treatment of obesity and diabetes, because the main toxicity of these ligands is related to its action in central nervous system [32].

2.3. DFT calculations

Several antioxidant mechanisms have been attributed to guaiacol derivatives and phenolic compounds such as HAT, Sequential Proton-Loss Electron Transfer (SPLET) and Single Electron Transfer (SET) [33]. Taking this into account, a DFT study was performed to propose a plausible mechanism of the antioxidant action of hybrids and gain greater understanding of the

Table 3
In vivo hypoglycemic activity (at 50 mg/kg) of compounds **1**, **2**, **4** and **12**.

Compound	Blood glucose-lowering profile at 7 h (mg/dL)[a]	% of change of glucose over control
1	−70.52 ± 10.19***	64.9
2	−32.35 ± 7.30	26.6
4	−39.00 ± 6.50*	33.3
12	−41.00 ± 7.10**	35.3

*p < 0.05; **p < 0.01, ***p < 0.001 as compared to untreated group. The negative value (−) indicates a decrease in glycemia compared with time 0.
[a] Values are represented as means ± SEM. (n = 5).

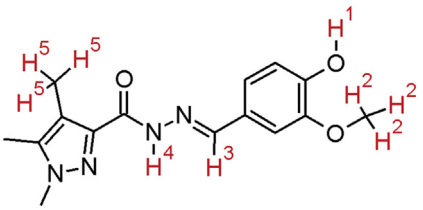

Fig. 7. Hydrogen atom numeration of virtual analog considered in the theoretical study.

phenomena. Several oxygen radicals with different electrophilic nature were explored, named $HO^{\bullet}$, $HOO^{\bullet}$, $CH_3OO^{\bullet}$, $CH_2CHOO^{\bullet}$ and $CCl_3OO^{\bullet}$ (in ascending electrophilic character); M06-2X functional in conjunction with the 6−31++G (d,p) basis set were used in the study, since it has been recommended for kinetic calculations by its developers [34].

Considering that the antioxidant effect is due to the phenolic moiety and not to the 1,5-diarylpyrazole ring (in accordance to the results found in the DPPH and ORAC tests), a virtual analog (Fig. 7) was modeled. This compound lacks of aromatic rings at 1 and 5 positions, which were substituted by methyl groups; however this reduction in atoms number was suitable for completing the study in reasonable time and also contained the structural features responsible of the DPPH and peroxyl radicals scavenging. Five possible removable hydrogen atoms were considered for both thermodynamic and kinetic determinations, labeled H^1, H^2, H^3, H^4 and H^5 (Fig. 7). The Gibbs free energy of the studied reaction paths involving hydrogen atom transfer are summarized in Table 4. As it can be shown, only the H^1 HAT pathway presented an exergonic behavior independently of the reactive radical tested, ranging from −2.88 to −35.43 kcal/mol. Other hydrogen atom transfer reactions that resulted in a viable path were the abstraction of the amide hydrogen and the hydrogen at methyl group in the pyrazole ring, which were found to be exergonic abstractions with either nucleophilic ($CH_3O^{\bullet}$) or electrophilic ($CCl_3OO^{\bullet}$) radicals.

Thermodynamic data showed above points that the abstraction of the H^1 trough a HAT pathway seems to be the main mechanism implicated in the antioxidant activity of compounds **1**–**13**. However, the kinetic of the reaction must also be considered, since a high reaction rate would conduct to a rapid products formation and thus could prevent cell damage caused by reactive radicals. The endergonic paths were not included because, even if they take place at a significant rate, the reversibility of the reaction will not

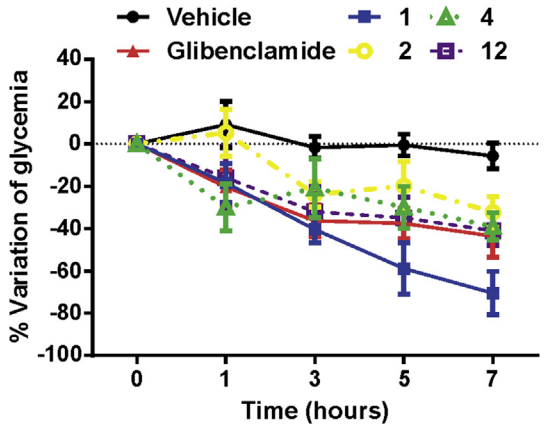

Fig. 6. Plasma glucose reduction after treatment with compounds **1**, **2**, **4** and **12** (50 mg/kg).

afford the products. We considered the H^1, H^2, H^3 and H^5 abstractions mediated by some radicals with different electrophilicity. The fully optimized geometries of the transition states (TS) are shown in Fig. 8. All the transition states corresponding to HAT from the phenolic OH (H^1 abstraction) showed a delocalization of the radical within the aromatic ring. This delocalization led to several canonical structures and results in stabilization of the transition states. This hypothesis can be corroborated in the $\Delta G^{\neq}$ of the transition states of the H^1 (Table 5), which are lower than those calculated for other hydrogen abstractions. For example, the $\Delta G^{\neq}$ for H^1 path by $CH_3O^{\bullet}$ was 11.50 kcal, whereas H^2, H^3 and H^5 showed higher $\Delta G^{\neq}$ values (15.89, 18.52 and 13.60 kcal, respectively). Similar results were found with the more electrophilic radical $Cl_3COO^{\bullet}$, in which the $\Delta G^{\neq}$ of H^1 path was found to be 2 kcal lower than the calculated for H^5 (11.81 kcal for H^1 versus 13.84 kcal for H^5). Therefore, it is expected that kinetics would favor the H^1 HAT over other possible and thermodynamically favored paths, such as H^5.

In addition, the rate constants of each reaction path are reported in Table 5. The calculated values of k range from 10^3 to 10^7 $M^{-1}s^{-1}$. When comparing the possible mechanisms for HAT by $CH_3O^{\bullet}$ radical, it is noteworthy that the H^1 path has the higher rate constant among them (8.42×10^7 $M^{-1}s^{-1}$), followed by the H^5 abstraction with k of 8.54×10^6 $M^{-1}s^{-1}$ and is ten-fold slower than H^1 entry. The same finding occurs with $Cl_3COO^{\bullet}$ radical, where H^1 abstraction was found to be more rapid than H^5 path. According to the latter, the most important mechanism that contributes to the antioxidant properties of compounds **1**–**13** is the HAT of the phenolic hydrogen (H^1) through a reaction that involves the generation of a stabilized phenoxyl radical, followed by the H^5 path, in which the homolytic cleavage at this position conduct to the formation of a benzyl-like radical. Notably, the rate constants obtained in this work are higher than those calculated for guaiacol derivatives, whose k values range from 10^2 to 10^4 in aqueous solution [35]. This is logical since the TS in compounds **1**–**13** have more resonance structures than guaiacol derivatives, in part, due to the extended double bond of the hydrazone moiety.

Furthermore, the SET mechanism was also studied for several radicals, albeit all the cases resulted in an endergonic reaction (Table 4). Previous works have demonstrated that this mechanism is not significant at physiological pH (pH = 7.4) in guaiacol analogs, in which almost all derivatives (such as eugenol, vanillic alcohol

Table 4
Gibbs free energies of reaction (kcal/mol) at 298.15 K for HAT and SET mechanisms.

Radical	HAT (kcal/mol)					SET (kcal/mol)
	H^1	H^2	H^3	H^4	H^5	
$HO^{\bullet}$	−35.43	−21.64	−15.31	−25.28	−28.35	8.12
$HOO^{\bullet}$	−3.29	10.50	16.83	6.86	3.79	30.74
$CH_3O^{\bullet}$	−20.16	−6.37	−0.04	−10.01	−13.08	24.19
$CH_3OO^{\bullet}$	−1.58	12.21	18.54	8.57	5.50	32.28
$CH_2CHOO^{\bullet}$	−2.88	10.91	17.24	7.27	4.20	26.13
$Cl_3COO^{\bullet}$	−11.00	2.80	9.12	−0.85	−3.92	9.78

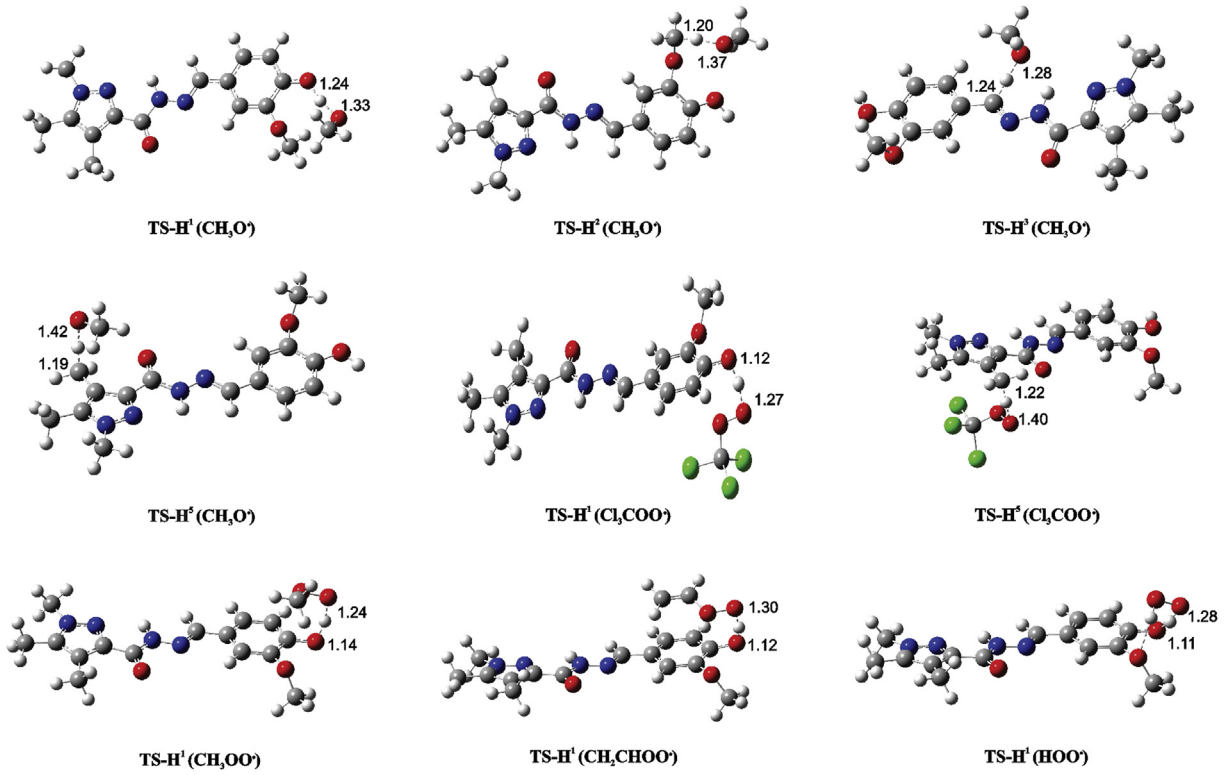

Fig. 8. Optimized geometries of the HAT transition states (the distances are expressed in Å).

and even guaiacol) are predominantly in its neutral state [36]. However, this mechanism becomes more important at basic pH values, where the antioxidant species are the phenoxide anions due to the known electro-donating capacity of this ion [35]. Accordingly, this process actually corresponds to a sequential proton loss electron transfer mechanisms (SPLET) that involves the electron transfer between the anion of the antioxidant and the radical and was first proposed by Litwinienko and Ingold [37–40]. Virtual analog was also employed in these calculations and its pKa value was estimated (pKa = 11.14; molar fraction of the phenoxide anion of 0.02 at physiologic pH). Considering the molar fraction, the calculated rate constants ranged from 10^5 to 10^8 and are higher than those obtained for HAT mechanism with except to the constant for HOO•, in which no significant difference was observed (Table 5). In conclusion, even though the deprotonated fraction is very low (i.e. 0.02), the rate constant of SPLET is faster than the HAT occurring in the neutral molecule of the antioxidant. Thus, both HAT at H^1 position and SPLET mechanisms contribute to a significant extent to the overall reactivity of compounds **1**–**13** toward radicals.

3. Conclusions

Considering the relationship between diabetes mellitus, oxidative stress and metabolic syndrome, thirteen hybrids of vanillin and CB1 antagonists were designed and synthesized. The design contemplated that the extension in conjugation of the π system in vanillin could increase the antioxidant activity of the guaiacol derivative. In this sense, hybrids **1**–**13** showed a significant antioxidant capacity in DPPH-scavenging and ORAC *in vitro* determinations. In the case of DPPH test, all the compounds exhibited a better scavenging effect than vanillin and vanillic acid, in which compound **7** was the most active (EC_{50} = 2.34 mM). On the other hand, the ORAC assay corroborated the previously observed results and indicated that hybrids had an antioxidant effect ranging from 401 to 1076 trolox equivalents/g of compound. In this case, compound **2** showed the best antioxidant capacity (1076 trolox equivalents). Although the *in vitro* antioxidant capacity was confirmed with these studies, structure-activity relationships could not be established since the antioxidant capacity is due to the guaiacol moiety.

Table 5
Gibbs free energies of activation and rate constants at 298.15 K.

Radical	SPLET	HAT		
	Rate constants ($M^{-1}s^{-1}$)	HAT pathway	$\Delta G^{\neq}$ (kcal/mol)	Rate constants ($M^{-1}s^{-1}$)
$CH_3O^•$	1.67×10^8	H^1	11.50	8.42×10^7
		H^2	15.89	3.78×10^5
		H^3	18.52	4.40×10^3
		H^5	13.61	8.54×10^6
$Cl_3COO^•$	1.53×10^8	H^1	11.81	2.70×10^7
		H^5	13.84	4.63×10^6
$CH_2CHOO^•$	1.45×10^8	H^1	15.58	5.47×10^5
$CH_3OO^•$	4.04×10^7	H^1	19.08	6.46×10^4
$HOO^•$	2.89×10^5	H^1	19.19	6.97×10^5

In addition, hybrids **1**, **2**, **4** and **12** were evaluated for its *in vivo* hypoglycemic effect in a DMTII model. Compounds presented a significant plasma glucose reduction at 7 h after administration; notably rimonabant hybrid **1** showed the higher effect with a decrease of 70%. In closing, with the information described above, the dual activity of compounds **1**–**13** was confirmed by presenting hypoglycemic activity as well as antioxidant properties.

Finally, the DFT thermodynamic and kinetic studies corroborated that the most feasible and rapid mechanism that contributes to the radical scavenging properties is the reaction of the phenolic hydrogen through a HAT path. However, at physiologic pH, in which there exists deprotonated species, the SPLET mechanism becomes the most probable mechanism. Gratifyingly, compounds **1**–**13** consolidate as new pyrazole leads with both hypoglycemic and antioxidant properties, which would further be used in the treatment and prophylaxis of diabetes and metabolic syndrome.

4. Experimental

4.1. Chemistry

Solvents and reagents were purchased from Sigma–Aldrich and were used without purification. Melting points were determined on a Büchi melting point apparatus, model B-540 and are uncorrected. The progress of reactions and the purity of final products were monitored by thin layer chromatography (TLC) whereas UV and iodine oxidation were used as revealing agents. ^{1}H and ^{13}C NMR spectra were obtained in DMSO-*d6* and $CDCl_3$ solutions at 400 MHz (for ^{1}H) and 100 MHz (for ^{13}C) on a Varian MR-400 (9.2 T) instrument and on a Varian VNMRS-400 (9.2 T) instrument. Chemical shifts (δ) are reported in ppm relative to the solvent signal.

Mass spectrometry spectra were obtained using a Thermoelectron model DFS instrument. Glibenclamide, nicotinamide, streptozotocin and Tween 80 were purchased from Sigma–Aldrich Co. (St. Louis, MO, USA).

4.1.1. General procedure for the synthesis of lithium salt of ethyl 3-methyl-2,4-dioxo-4-phenylbutanoates (**14**–**18**)

A solution of the corresponding propiophenone (15.06 mmol) in 3 mL of anhydrous methylcyclohexane was added at room temperature to a magnetically stirred solution of lithium bis(-trimethylsilyl)amide (16.1 mmol) in anhydrous methylcyclohexane (3–5 mL). After 3 h of stirring, diethyl oxalate (16.6 mmol) was added dropwise and then left to react for 16 h. The mixture was filtered and washed with several portions of methylcyclohexane and used in the next reaction without purification.

*4.1.1.1. Lithium salt of ethyl 3-methyl-2,4-dioxo-phenylbutanoate (**14**).* Yellow solid in 97% yield.

*4.1.1.2. Lithium salt of ethyl 4-(4-chlorophenyl)-3-methyl-2,4-dioxobutanoate (**15**).* Yellow solid in 89% yield.

*4.1.1.3. Lithium salt of ethyl 4-(4-fluorophenyl)-3-methyl-2,4-dioxobutanoate (**16**).* Yellow solid in 93% yield.

*4.1.1.4. Lithium salt of ethyl 3-methyl-2,4-dioxo-4-[4-(trifluoromethyl)phenyl]butanoate (**17**).* Yellow solid in 70% yield.

*4.1.1.5. Lithium salt of ethyl 4-(4-bromophenyl)-3-methyl-2,4-dioxobutanoate (**18**).* Yellow solid in 60% yield.

4.1.2. General procedure for the synthesis of 1,5-diarylpyrazole-3-carboxylic acids (**19**–**31**)

A mixture of the lithium salt of the corresponding ethyl 3-methyl-2,4-dioxo-4-phenylbutanoate (13.8 mmol) and substituted phenylhydrazine (15.6 mmol) was suspended in 50 mL of EtOH and H_2SO_4 was added dropwise in an ice bath. The mixture was heated to reflux and stirred until the starting material was completely consumed. The resulting solution was cooled to room temperature and the excess of ethanol was removed *in vacuo*. 20 mL of water were added and the suspension was neutralized with $NaHCO_3$ and then extracted with $CHCl_3$ (3 × 20 mL). The organic layer was successively dried over Na_2SO_4, filtered and concentrated *in vacuo*. The residue containing the ester product was then dissolved in 20 mL of EtOH and KOH (23 mmol) was added. The mixture was allowed to react 12 h at 50 °C. The resulting suspension was concentrated *in vacuo* and dissolved in 30 mL of water and later washed with hexane (3 × 15 mL). The aqueous layer was acidified with concentrated HCl until the pure carboxylic acids precipitated.

*4.1.2.1. 5-(4-Chlorophenyl)-1-(2,4-dichlorophenyl)-4-methyl-1H-pyrazole-3-carboxylic acid (**19**).* Beige solid in 87% yield, mp 208–210 °C. FAB-MS *m/z* 381 [(M+1)+], 383 [(M+3)+], 385 [(M+5)+], 363[(M+1)-18]. ^{1}H NMR (400 MHz, DMSO-d_6): δ 7.77 (d, J = 2.0 Hz, 1H, ArH), 7.69 (d, J = 8.4 Hz, 1H, ArH), 7.56 (dd, J = 8.8 y 2.4 Hz, 1H, ArH), 7.44 (d, J = 8.4 Hz, 2H, ArH), 7.21 (d, J = 8.4 Hz, 2H, ArH), 2.23 (s, 3H, CH_3).

*4.1.2.2. 1-(2,4-Dichlorophenyl)-4-methyl-5-phenyl-1H-pyrazole-3-carboxylic acid (**20**).* Light brown solid in 68% yield, mp 189–191 °C. EI-MS m/z 346 [M+], 348 [(M+2)+]. ^{1}H NMR (300 MHz, DMSO-d_6): δ 12.95 (bs, 1H, ArCOOH), 7.77 (d, J = 2.1 Hz, 1H, ArH), 7.69 (d, J = 8.4 Hz, 1H, ArH), 7.56 (dd, J = 8.6 and 2.1 Hz, 1H, ArH), 7.41–7.34 (m, 3H, ArH), 7.22–7.19 (m, 3H, ArH), 2.23 (s, 3H, CH_3).

*4.1.2.3. 4-Methyl-1,5-diphenyl-1H-pyrazole-3-carboxylic acid (**21**).* Yellowish solid in 74% yield, mp 256–258 °C. FAB-MS m/z 279 [(M+1)+], 261 [(M+1)-18], 233 [(M+1)-46]. ^{1}H NMR (300 MHz, DMSO-d_6): δ 7.44–7.26 (m, 6H, ArH), 7.23–7.18 (m, 4H, ArH), 2.20 (s, 3H, CH_3).

*4.1.2.4. 5-(4-Chlorophenyl)-1-(3,4-dichlorophenyl)-4-methyl-1H-pyrazole-3-carboxylic acid (**22**).* Light brown solid in 82% yield, mp 203–204 °C. FAB-MS m/z 381 [(M+1)+], 383 [(M+3)+], 385 [(M+5)+], 363[(M+1)-18]. ^{1}H NMR (300 MHz, DMSO-d_6): δ 7.85 (d, J = 2.4 Hz, 1H, ArH), 7.67 (d, J = 8.7 Hz, 1H, ArH), 7.56 (d, J = 8.4 Hz, 2H, ArH), 7.36 (d, J = 8.4 Hz, 2H, ArH), 7.14 (dd, J = 8.8 and 2.4 Hz, 1H, ArH), 2.21 (s, 3H, CH_3).

*4.1.2.5. 1-(3-Chloro-4-fluorophenyl)-5-(4-chlorophenyl)-4-methyl-1H-pyrazole-3- carboxylic acid (**23**).* Light brown solid in 75% yield, mp 169–171 °C. FAB-MS m/z 365 [(M+1)+], 367 [(M+3)+], 347 [(M+1)-18]. ^{1}H NMR (300 MHz, DMSO-d_6): δ 7.6 (dd, J = 6.6 and 2.7 Hz, 1H, ArH), 7.50 (d, J = 8.4 Hz, 2H, ArH), 7.44 (t, J = 9.0 Hz, 1H, ArH), 7.28 (d, J = 8.7 Hz, 2H, ArH), 7.19–7.14 (m, 1H, ArH), 2.19 (s, 3H, CH_3).

*4.1.2.6. 5-(4-Chlorophenyl)-1-(7-chloroquinolin-4-yl)-4-methyl-1H-pyrazole-3- carboxylic acid (**24**).* Yellow solid in 51% yield, mp 221–223 °C. FAB-MS m/z 398 [(M+1)+], 400 [(M+3)+], 401 [(M+5)+], 380 [(M+1)-18]. ^{1}H NMR (300 MHz, DMSO-d_6): δ 8.98 (d, J = 4.5 Hz, 1H, ArH), 8.78 (d, J = 1.8 Hz, 1H, ArH), 7.71–7.62 (m 2H, ArH), 7.53 (d, J = 4.5 Hz, 1H, ArH), 7.36 (d, J = 8.7 Hz, 2H, ArH), 7.20 (d, J = 8.4 Hz, 2H, ArH), 2.27 (s, 3H, CH_3).

*4.1.2.7. 5-(4-Chlorophenyl)-4-methyl-1-[4-(trifluoromethyl)phenyl]-1H-pyrazole-3-carboxylic acid (**25**).* Light brown solid in 59% yield, mp 199–200 °C. ^{1}H NMR (300 MHz, DMSO-d_6): δ 13.03(bs, 1H, ArCOOH), 7.79 (d, J = 8.4 Hz, 2H, ArH), 7.52 (d, J = 8.7 Hz, 2H, ArH), 7.46 (d, J = 8.1 Hz, 2H, ArH), 7.30 (d, J = 8.7 Hz, 2H, ArH), 2.20 (s, 3H, CH_3).

*4.1.2.8. 1-(2,4-Difluorophenyl)-5-(4-fluorophenyl)-4-methyl-1H-pyrazole-3-carboxylic acid (**26**).* White solid in 50% yield, mp 190–191 °C. FAB-MS m/z 333 [(M+1)+], 315 [(M+1)-18], 287 [(M+1)-46]. ^{1}H NMR (300 MHz, DMSO-d_6): δ 12.92 (bs, 1H, ArCOOH), 7.73–7.65 (m, 1H, ArH), 7.45–7.37 (m, 1H, ArH), 7.30–7.20 (m, 5H, ArH), 2.21 (s, 3H, CH_3).

*4.1.2.9. 1-(3-Chloro-4-fluorophenyl)-5-(4-fluorophenyl)-4-methyl-1H-pyrazole-3-carboxylic acid (**27**).* Light brown solid in 68% yield, mp 167–168 °C. FAB-MS m/z 349 [(M+1)+], 351 [(M+3)+], 331 [(M+1)-18].]. ^{1}H NMR (300 MHz, DMSO-d_6): δ 12.98 (bs, 1H, ArCOOH), 7.59 (dd, J = 6.6 and 2.7 Hz, 1H, ArH), 7.45 (t, J = 9.0 Hz, 1H, ArH), 7.35–7.25 (m, 4H, ArH), 7.22–7.16 (m, 1H, ArH), 2.18 (s, 3H, CH_3).

*4.1.2.10. 1-(7-Chloroquinolin-4-yl)-5-(4-fluorophenyl)-4-methyl-1H-pyrazole-3-carboxylic acid (**28**).* Light brown solid in 73% yield, mp 185–186 °C. FAB-MS m/z 382 [(M+1)+], 384 [(M+3)+], 364 [(M+1)-18]. ^{1}H NMR (300 MHz, DMSO-d_6): δ 8.98 (d, J = 4.5 Hz, 1H, ArH), 8.20 (bs, 1H, ArH), 7.67 (d, J = 1.2 Hz, 1H, ArH), 7.50 (d, J = 4.5 Hz, 1H, ArH), 7.34–7.23 (m, 3H, ArH), 7.18–7.12 (m, 2H, ArH), 2.29 (s, 3H, CH_3).

*4.1.2.11. 5-(4-Bromophenyl)-4-methyl-1-[4-(trifluoromethyl) phenyl]-1H-pyrazole-3-carboxylic acid (**29**).* Yellow solid in 60% yield, mp 171–173 °C. ^{1}H NMR (300 MHz, DMSO-d_6): δ 13.03 (bs, 1H, ArCOOH), 7.80 (d, J = 8.4 Hz, 2H, ArH), 7.52 (d, J = 8.7 Hz, 2H, ArH), 7.46 (d, J = 8.4 Hz, 2H, ArH), 7.45 (d, J = 8.4 Hz, 2H, ArH), 2.20 (s, 3H, CH_3).

*4.1.2.12. 1-(2,4-Dichlorophenyl)-4-methyl-5-[4-(trifluoromethyl) phenyl]-1H-pyrazole-3-carboxylic acid (**30**).* Light orange solid in 81% yield, mp 156–158 °C. FAB-MS m/z 415 [(M+1)+], 417 [(M+3)+], 397 [(M+1)-18]. ^{1}H NMR (300 MHz, DMSO-d_6): δ 7.82 (d, J = 2.4 Hz, 1H, ArH), 7.79 (d, J = 8.1 Hz, 2H, ArH), 7.76 (d, J = 8.7 Hz, 1H, ArH), 7.61 (dd, J = 8.6 and 2.4 Hz, 1H, ArH), 7.46 (d, J = 7.8 Hz, 2H, ArH), 2.29 (s, 3H, CH_3).

*4.1.2.13. 1-(2,4-Difluorophenyl)-4-methyl-5-[4-(trifluoromethyl) phenyl]-1H-pyrazole-3-carboxylic acid (**31**).* Light brown solid in 59% yield, mp 198–199 °C. ^{1}H NMR (300 MHz, DMSO-d_6): δ 13.03 (bs, 1H, ArCOOH), 7.78 (d, J = 8.4 Hz, 2H, ArH), 7.75–7.69 (m, 1H, ArH), 7.46 (d, J = 8.1 Hz, 2H, ArH), 7.44–7.40 (m, 1H, ArH), 7.30–7.23 (m, 1H, ArH), 2.25 (s, 3H, CH_3).

*4.1.3. General procedure for the synthesis of N′-[(Z)-(4-hydroxy-3-methoxyphenyl)methylidene]-4-methyl-1H-pyrazole-3-carbohydrazides (**1**–**3**)*

To a stirred solution of 0.5 mmol of the corresponding 1,5-diarylpyrazole-3-carboxylic acid (**19**–**31**) in 15 mL of toluene, 0.2 mL of $SOCl_2$ was slowly added. The mixture was heated to reflux for ca. 2.5 h. Then, the excess of solvent and $SOCl_2$ was removed *in vacuo* and the residue was dissolved in 10 mL of $CHCl_3$. To this stirred mixture at 0 °C, a solution of 0.55 mmol of *t*-butyl carbazate and 0.55 mmol of diisopropylethylamine (DIPEA) was added dropwise. After the consumption of the acyl chloride, the chloroformic solution was subsequently washed with citric acid 0.5 M and saturated aqueous $NaHCO_3$. The combined organic extracts were filtered, dried over Na_2SO_4 and evaporated, which afforded the desired *N*-Boc carbohydrazides in an acceptable purity.

The unpurified *N*-Boc carbohydrazides were stirred with 1 mL of TFA at room temperature for 2.5 h. Once the deprotection was completed, the remnant TFA was co-distilled with 20 mL of $CHCl_3$ (this procedure was repeated two more times). Finally, to the resulting oil 20 mL of $CHCl_3$ were added and 0.55 mmol of vanillin and catalytic acetic acid were aggregated. The solution was stirred for ca. 4 h at room temperature and then evaporated. The solid was purified by column chromatography on silica gel ($CHCl_3$ to $CHCl_3$–MeOH 9:1) to afford the desired carbohydrazydes **1**–**13**.

*4.1.3.1. 5-(4-Chlorophenyl)-1-(2,4-dichlorophenyl)-N′-[(Z)-(4-hydroxy-3-methoxyphenyl)methylidene]-4-methyl-1H-pyrazole-3-carbohydrazide (**1**).* White solid in 68% yield; mp 256–258 °C. ^{1}H NMR (400 MHz, DMSO-d_6): δ 2.29 (s, 3H, CH_3), 3.83 (s, 3H, OCH_3), 6.83 (d, J = 8 Hz, 1H, ArH), 7.02 (dd, 1H, J = 8 and 2 Hz, ArH), 7.27 (d, J = 8.4 Hz, 2H, ArH), 7.29 (d, J = 2 Hz, 1H, ArH), 7.47 (d, J = 8.8 Hz, 2H, ArH), 7.60 (dd, J = 8.6 and 2.4 Hz, 1H, ArH), 7.78 (d, J = 1.6 Hz, 1H, ArH), 7.79 (d, J = 8.8 Hz, 1H, ArH), 8.40 (s, 1H, NCH), 9.53 (s, 1H, ArOH), 11.60 (s, 1H, CO NH).^{13}C NMR (100 MHz, DMSO- d_6): δ 9.6, 56.0, 109.2, 115.8, 117.6, 122.6, 126.4, 127.6, 128.8, 129.2, 130.1, 131.8, 132.4, 132.6, 134.3, 135.6, 136.1, 143.1, 144.4, 148.5, 148.8, 149.4, 158.6. FTIR (cm^{-1}): 3536.96, 3166.88, 3075.88, 2984.14, 2941.87, 1645.54, 1602.45, 1508.51, 1387.98, 1266.22, 1116.45. FAB-MS (m/z): 529 [(M+1)]+ 531 [(M+2)]+. HRFAB-MS m/z 528.0504 (calcd for $C_{25}H_{19}O_3N_4^{35}Cl_3$: 528.0517).

*4.1.3.2. 1-(2,4-Dichlorophenyl)-N′-[(Z)-(4-hydroxy-3-methoxyphenyl)methylidene]-4-methyl-5-phenyl-1H-pyrazole-3-carbohydrazide (**2**).* Beige solid in 69% yield; mp 239–241 °C. ^{1}H NMR (400 MHz, DMSO-d_6): δ 2.29 (s, 3H, CH_3), 3.83 (s, 3H, OCH_3), 6.83 (d, J = 8 Hz, 1H, ArH), 7.01 (dd, 1H, J = 8.2 and 2 Hz, ArH), 7.25–7.22 (m, 2H, ArH), 7.28 (d, J = 2 Hz, 1H, ArH), 7.41–7.34 (m, 3H, ArH), 7.60 (dd, J = 8.6 and 2.4 Hz, 1H, ArH), 7.76 (d, J = 2.4 Hz, 1H, ArH), 7.76 (d, J = 8.4 Hz, 1H, ArH), 8.40 (s, 1H, NCH), 9.52 (s, 1H, ArOH), 11.60 (s, 1H, CONH). ^{13}C NMR (100 MHz, DMSO-d_6): δ 9.2, 55.5, 108.7, 115.4, 115.4, 122.1, 125.9, 128.19, 128.2, 128.6, 128.9, 129.51, 129.54, 132.0, 132.4, 135.0, 135.9, 143.85, 143.89, 148.0, 148.2, 148.9, 158.3. FTIR (cm^{-1}): 3534.50, 3171.42, 3074.21, 1646.31, 1603.29, 1509.33, 1384.44, 1273.69, 1095.86. EI-MS m/z 494 [M+]. HREI–MS = 494.0900 (calcd for $C_{25}H_{20}O_3N_4^{35}Cl_2$: 494.0907).

*4.1.3.3. N′-[(Z)-(4-hydroxy-3-methoxyphenyl)methylidene]-4-methyl-1,5-diphenyl-1H-pyrazole-3-carbohydrazide (**3**).* White solid in 62% yield; mp 291–292 °C. ^{1}H NMR (400 MHz, DMSO-d_6): δ 2.25 (s, 3H, CH_3), 3.84 (s, 3H, OCH_3), 6.84 (d, J = 8 Hz, 1H, ArH), 7.04 (dd, 1H, J = 8.2 and 2 Hz, ArH), 7.28–7.23 (m, 2H, ArH), 7.34–7.29 (m, 3H, ArH), 7.45–7.36 (m, 6H, ArH), 8.40 (s, 1H, NCH), 9.52 (s, 1H, ArOH), 11.52 (s, 1H, CONH). ^{13}C NMR (100 MHz, DMSO-d_6): δ 9.1, 55.5, 108.8, 115.4, 117.7, 122.1, 125.3, 125.9, 128.0, 128.7, 128.7, 128.9, 129.1, 129.9, 139.2, 142.0, 143.3, 148.03, 148.05, 148.9, 158.5 FTIR (cm^{-1}): 3312.93, 3070.81, 3013.47, 2955.54, 2929.85, 1678.17, 1598.83, 1513.97, 1362.82, 1268.20, 1117.05. FAB-MS m/z 427 [(M+1)]+.HRFAB-MS = 427.1738 (calcd for $C_{25}H_{23}O_3N_4$: 427.1765).

*4.1.3.4. 5-(4-Chlorophenyl)-1-(3,4-dichlorophenyl)-N′-[(Z)-(4-hydroxy-3-methoxyphenyl)methylidene]-4-methyl-1H-pyrazole-3-carbohydrazide (**4**).* White solid in 60% yield; mp 224–225 °C. ^{1}H NMR (400 MHz, DMSO-d_6): δ 2.23 (s, 3H, CH_3), 3.84 (s, 3H, OCH_3), 6.85 (d, J = 8.4 Hz, 1H, ArH), 7.06 (dd, 1H, J = 8.2 and 2.0 Hz, ArH), 7.14 (dd, J = 8.8 and 2.4 Hz, 1H, ArH), 7.32 (d, J = 2.4 Hz, 1H, ArH), 7.34 (d, J = 8.4, 2H, ArH), 7.54 (d, J = 8.4 Hz, 2H, ArH), 7.66 (d, J = 8.8 Hz, 1H, ArH), 7.81 (d, J = 2.4 Hz, 1H, ArH), 8.40 (s, 1H, NCH), 9.54 (s, 1H, ArOH), 11.60 (s, 1H, CONH). ^{13}C NMR (100 MHz, DMSO-

d_6): δ 8.9, 55.5, 108.8, 115.4, 118.6, 122.2, 124,8, 125.8, 126.9, 127.4, 129.0, 130.5, 130.8, 131,6, 131.8, 134.0, 138.6, 140.8, 144.0, 148.1, 148.3, 149.0, 158.1. FTIR (cm^{-1}): 3538.62, 3249.38, 3098.37, 2925.57, 1655.38, 1599.43, 1509.20, 1363.81, 1268.71, 1127.16. FAB-MS m/z 529 [(M+1)]. HRFAB-MS = 528.0464 (calcd for $C_{25}H_{19}O_3N_4^{35}Cl_3$: 528.0517).

*4.1.3.5. 1-(3-Chloro-4-fluorophenyl)-5-(4-chlorophenyl)-N′-[(Z)-(4-hydroxy-3-methoxyphenyl)methylidene]-4-methyl-1H-pyrazole-3-carbohydrazide (**5**).* White solid in 62% yield; mp 210–212 °C. ^{1}H NMR (400 MHz, DMSO-d_6): δ 2.24 (s, 3H, CH_3), 3.84 (s, 3H, OCH_3), 6.84 (d, J = 8.0 Hz, 1H, ArH), 7.05 (dd, 1H, J = 8.2 and 1.6 Hz, ArH), 7.21–7.17 (m, 1H, ArH), 7.34–7.31 (m, 3H, ArH), 7.46 (t, J = 9.2 Hz, 1H, ArH), 7.53 (d, J = 8.8 Hz, 2H, ArH), 7.78 (dd, J = 6.6 and 2.8 Hz, 1H, ArH), 8.41 (s, 1H, NCH), 9.52 (s, 1H, ArOH), 11.56 (s, 1H, CONH).^{13}C NMR (100 MHz, DMSO-d_6): δ 9.0, 55.5, 108.8, 115.4, 117.1 (d, J = 22.4 Hz), 118.3, 119.9 (d, J = 18.9 Hz), 122.2, 125.8, 125.9 (d, J = 7.6 Hz), 127.4, 127.7, 128.9, 131.9, 133.9, 136.0 (d, J = 3.5 Hz), 141.0, 143.7, 148.0, 148.2, 148.9, 156.5 (d, J = 247.1 Hz), 158.2. FTIR (cm^{-1}): 3328.45, 3192.15, 3102.37, 2997.81, 1665.44, 1594.39, 1520.10, 1390.39, 1267.18, 1123.19. EI-MS m/z 512(M+). HREI–MS = 512.0801 (calcd for $C_{25}H_{19}O_3N_4^{35}Cl_2F_1$: 512.0801).

*4.1.3.6. 5-(4-Chlorophenyl)-1-(7-chloroquinolin-4-yl)-N'-[(Z)-(4-hydroxy-3-methoxyphenyl)methylidene-4-methyl-1H-pyrazole-3-carbohydrazide (**6**).* Yellowish solid in 59% yield; mp 272–273 °C. ^{1}H NMR (400 MHz, DMSO-d_6): δ 2.35 s, 3H, CH_3), 3.83 (s, 3H, OCH_3), 6.83 (d, J = 8 Hz, 1H, ArH), 7.01 (dd, J = 8.2 and 2 Hz, 1H, ArH), 7.25 (d, J = 8.8 Hz, 2H, ArH), 7.29 (d, J = 2 Hz, 1H, ArH), 7.39 (d, J = 8.4, 2H, ArH), 7.56 (d, J = 4.8 Hz, 1H, ArH), 7.68 (dd, J = 8.8 and 2.4 Hz, 1H, ArH), 7.77 (d, J = 8.8 Hz, 1H, ArH), 8.21 (d, J = 2.4, 1H, ArH), 8.36 (s, 1H, NCH), 8.99 (d, J = 4.8 Hz, 1H, ArH), 9.54 (s, 1H, ArOH), 11.61 (s, 1H, CONH). ^{13}C NMR (100 MHz, DMSO-d_6): δ 9.1, 55.5, 108.8, 115.4, 118.1, 120.5, 122.2, 122.6, 125.77, 125.79, 127.0, 127.9, 128.7, 128.4, 131.3, 133.9, 135.2, 142.9, 143.0, 144.8, 148.0, 148.5, 149.0, 149.2, 152.1, 158.1. FTIR (cm^{-1}): 3476.13, 3318.50, 3083.09, 2995.49, 2933.60, 1686.83, 1657.82, 1508.35, 1377.15, 1267.85 1123.72. EI-MS m/z 545 (M+). HR–EIMS = 545.0988 (calcd for $C_{28}H_{21}O_3N_5^{35}Cl_2$: 545.1016).

*4.1.3.7. 5-(4-Chlorophenyl)-N′-[(Z)-(4-hydroxy-3-methoxyphenyl) methylidene]-4-methyl-1-[4-(trifluoromethyl)phenyl]-1H-pyrazole-3-carbohydrazide (**7**).* Yellowish solid in 51% yield; mp 184–185 °C. ^{1}H NMR (400 MHz, DMSO-d_6): δ 2.24 (s, 3H, CH_3), 3.83 (s, 3H, OCH_3), 6.84 (d, J = 8 Hz, 1H, ArH), 7.05 (dd, J = 8.2 and 2 Hz, 1H, ArH), 7.34–7.31 (m, 3H, ArH), 7.55–7.52 (m, 4H, ArH), 7.82 (d, J = 8.4 Hz, 2H, ArH), 8.40 (s, 1H, NCH), 9.59 (s, 1H, ArOH), 11.62 (s, 1H, CONH). ^{13}C NMR (100 MHz, DMSO-d_6): δ 9.0, 55.6, 108.8, 115.5, 118.8, 122.3, 123.9 (q, J = 270.9 Hz), 125.6, 125.9, 126.4 (q, J = 3.7 Hz), 127.6, 128.1 (q, J = 32 Hz), 129.1, 131.9, 134.0, 140.9, 142.6, 144.3, 149.0, 148.4. FTIR (cm^{-1}): 3540.09, 3229.39, 3003.76, 2968.36, 2626.63, 1655.82, 1601.41, 1509.62, 1364.30, 1268.58, 1112.02. EI-MS m/z 528 (M+). HREI–MS = 528.1197 (calcd for $C_{26}H_{20}O_3N_4^{35}Cl_1F_3$: 528.1171).

*4.1.3.8. 1-(2,4-Difluorophenyl)-5-(4-fluorophenyl)-N′-[(Z)-(4-hydroxy-3-methoxyphenyl)methylidene]-4-methyl-1H-pyrazole-3-carbohydrazide (**8**).* Light pink solid in 57% yield; mp 241–242 °C. ^{1}H NMR (400 MHz, DMSO-d_6): δ 2.27 (s, 3H, CH_3), 3.83 (s, 3H, OCH_3), 6.83 (d, J = 8.4 Hz,1H, ArH), 7.02 (d, J = 8.2 y 1.6 Hz, 1H, ArH), 7.33–7.23 (m, 6H, ArH), 7.44–7.39 (m, 1H, ArH), 7.80–7.74 (m, 1H, ArH), 8.39 (s, 1H, NCH), 9.53 (s, 1H, ArOH), 11.60 (s, 1H, CONH). ^{13}C NMR (100 MHz, DMSO-d_6): δ 9.1, 55.6, 105.05 (dd, J = 28.6 and 23.7 Hz), 108.8, 112.3 (dd, J = 21.4 and 1.8 Hz), 115.4, 115.8 (d, J = 21.5 Hz), 117.1, 122.2, 123.7 (dd J = 12.3 and 3.6 Hz), 124.7 (d, J = 3.1 Hz), 125.9, 131.3 (d, J = 10.6 Hz), 131.7 (d, J = 8.6 Hz), 143.0, 144.1, 148.1, 148.2, 148.9, 156.4 (dd, J = 251.7 and 13.4 Hz), 158.3, 162.2 (d, J = 245.7 Hz), 162.2(dd, J = 248.7 and 11.5 Hz). FTIR (cm^{-1}): 3414.35, 3075.77, 3011.08, 2934.67, 1668.47, 1640.86, 1589.86, 1267.15, 1140.04. FAB-MS m/z 481 [(M+1)]+. HRFAB-MS = 481.1468 (calcd for $C_{25}H_{20}O_3N_4F_3$: 481.1482).

*4.1.3.9. 1-(3-Chloro-4-fluorophenyl)-5-(4-fluorophenyl)-N′-[(Z)-(4-hydroxy-3-methoxyphenyl)methylidene]-4-methyl-1H-pyrazole-3-carbohydrazide (**9**).* Yellowish solid in 84% yield; mp 206–207 °C. ^{1}H NMR (400 MHz, DMSO-d_6): δ 2.23 (s, 3H, CH_3), 3.84 (s, 3H, OCH_3), 6.84 (d, J = 8 Hz, 1H, ArH), 7.05 (dd, J = 8.2 and 2 Hz, 1H, ArH), 7.21–7.17 (m, 1H, ArH), 7.37–7.28 (m, 5H, ArH), 7.44 (t, J = 8.8. Hz, ArH), 7.74 (dd, J = 6.6 and 2.4 Hz, 1H, ArH), 8.41 (s, 1H, NCH), 9.55 (s, 1H, ArOH), 11.60 (s, 1H, CONH). ^{13}C NMR (100 MHz, DMSO-d_6): δ 9.0, 55.6, 108.8, 115.4, 116.0 (d, J = 21.6 Hz), 117.1 (d, J = 22.3 Hz), 118.2, 119.9 (d, J = 19.0 Hz), 122.2, 125.0 (d, J = 3.0 Hz), 125.8 (d, J = 8.2 Hz), 125.8, 127.6, 132.4 (d, J = 8.5 Hz), 136.1 (d, J = 3.3 Hz), 141.3, 143.6, 148.1, 148.3, 149.0, 156.5 (d, J = 247.3 Hz), 158.3, 162.3 (d, J = 245.8 Hz). FTIR (cm^{-1}): 3326.20, 3224.58, 3104.14, 2997.21, 2933.401666.29, 1592.75, 1508.95, 1389.50, 1266.92, 1122.41. FAB-MS m/z 497 [(M+1)]+. HRFAB-MS = 497.1168 (calcd for $C_{25}H_{20}O_3N_4^{35}Cl_1F_2$: 497.1187).

*4.1.3.10. 1-(7-Chloroquinolin-4-yl)-5-(4-fluorophenyl)-N′-[(Z)-(4-hydroxy-3-methoxyphenyl)methylidene]-4-methyl-1H-pyrazole-3-carbohydrazide (**10**).* Light brown solid in 55% yield; mp 289–291 °C. ^{1}H NMR (400 MHz, DMSO-d_6): δ 2.34 (s, 3H, CH_3), 3.83 (S, 1H, OCH_3), 6.83 (d, J = 8 Hz, 1H, ArH), 7.02 (dd, J = 8.2 and 2 Hz, 1H, ArH), 7.17 (t, J = 8.8 Hz, 2H, ArH), 7.29–7.27 (m, 2H, ArH), 7.30 (d, J = 2 Hz, 1H, ArH) 7.56 (d, J = 4.4 Hz, 1H; ArH), 7.67 (dd, J = 8.8 and 2.0 Hz, 1H, ArH), 7.75 (d, J = 9.2 Hz, 1H, ArH), 8.19 (d, J = 2.0 Hz, 1H, ArH), 8.36 (s, 1H, NCH), 8.99 (d, J = 4.4 Hz, 1H, ArH), 9.54 (s, 1H; ArOH), 11.60 (s, 1H, CONH). ^{13}C NMR (100 MHz, DMSO-d_6): δ 9.2, 55.6, 108.8, 115.4, 115.9 (d, J = 21.7 Hz), 118.0, 120.5, 122.2, 122.7, 124.6 (d, J = 3.2 Hz), 125.8, 128.0, 128.7, 131.9 (d, J = 8.5 Hz), 135.2, 143.2, 143.3, 144.7, 148.1, 148.5, 149.0, 149.2, 152.1, 158.3, 162.2 (d, J = 245.8 Hz). FTIR (cm^{-1}): 3322.91, 3027.77, 2930.55, 2899.02, 1733.92, 1629.44, 1572.84, 1375.65, 1239.29, 1124.76. EI-MS m/z 529 (M+). HRE–MS = 529.1300 (calcd para $C_{28}H_{21}O_3N_4^{35}Cl_1F_1$: 529.1300.

*4.1.3.11. 5-(4-Bromophenyl)-N′-[(Z)-(4-hydroxy-3-methoxyphenyl) methylidene]-4-methyl-1-[4-(trifluoromethyl)phenyl]-1H-pyrazole-3-carbohydrazide (**11**).* Brown solid in 78% yield; mp 289–290 °C. ^{1}H NMR (400 MHz, DMSO-d_6): δ 2.24 (s, 3H, CH_3), 3.84 (s, 3H, OCH_3), 6.84 (d, J = 7.8 Hz, 1H, ArH), 7.05 (dd, J = 8.1 and 1.8 Hz, 1H, ArH), 7.26 (d, J = 8.7 Hz, 2H, ArH), 7.32 (d, J = 1.8 Hz, 1H, ArH), 7.55 (d, J = 8.4 Hz, 1H, ArH), 7.67 (d, J = 8.4 Hz, 2H, ArH), 7.82 (d, J = 8.4 Hz, 1H, ArH), 8.40 (s, 1H, NCH), 9.59 (s, 1H, ArOH), 11.62 (s, 1H, CONH). ^{13}C NMR (100 MHz, DMSO-d_6): δδ 9.0, 55.6, 108.9, 115.5, 118.8, 122.3, 122.7, 123.9 (q, J = 270.9 Hz), 125.6, 125.8, 126.4 (q, J = 3.3 Hz), 128.0, 128.1 (q, J = 32.1 Hz), 132.0, 132.1, 140.9, 142.1, 144.3, 148.1, 148.4, 149.0, 158.3. FTIR (cm^{-1}): 3543.35, 3211.82 3073.59, 2965.49, 2932.88, 1654.58, 1614.70, 1510.35, 1363.40, 1269.03, 1115.34. EI-MS m/z 572 (M+). HR–EMEI = 572.0642 (calcd for $C_{26}H_{20}O_3N_4^{79}Br_1F_3$: 572.0665).

*4.1.3.12. 1-(2,4-Dichlorophenyl)-N′-[(Z)-(4-hydroxy-3-methoxyphenyl)methylidene]-4-methyl-5-[4-(trifluoromethyl) phenyl]-1H-pyrazole-3-carbohydrazide (**12**).* Light pink solid in 76% yield; 250–251 °C. ^{1}H NMR (400 MHz, DMSO-d_6): δ 2.23 (s, 3H, CH_3), 3.83 (s, 3H, OCH_3), 6.83 (d, J = 8.4 Hz, 1H, ArH), 7.02 (dd, J = 8.4 and 2 Hz, 1H, ArH), 7.30 (d, J = 2 Hz, 1H, ArH), 7.49 (d, J = 8.0 Hz, 2H, ArH), 7.62 (dd, J = 8.4 and 2.4 Hz, 1H, ArH), 7.78 (d, J = 8.8 Hz, 2H,

ArH), 7.80 (d, $J = 2$ Hz, 1H, ArH), 7.83 (d, $J = 8.4$ Hz, 1H, ArH), 8.40 (s, 1H, NCH), 9.53 (s, 1H, ArOH), 11.6 (s, 1H, CONH). δ. ^{13}C NMR (100 MHz, DMSO-d_6): δ 9.1, 55.5, 108.8, 115.4, 117.7, 122.2, 123.9 (q, $J = 270.7$ Hz), 125.6 (q, $J = 3.8$ Hz), 125.9, 128.4, 129.1 (q, $J = 31.9$ Hz), 129.7, 130.4, 132.0, 132.1, 132.4, 135.3, 135.6, 142.4, 144.1, 148.0, 148.4, 148.9, 158.1. FTIR (cm^{-1}): 3240.65, 3097.74, 3044.12, 2969.86, 2936.80, 1640.40, 1583.88, 1516.88, 1376.32, 1263.22, 1124.64. FAB-MS m/z 563(M+). HRFAB-MS = 563.0875 (calcd for $C_{26}H_{20}O_3N_4^{35}Cl_2F_3$: 563.0859).

*4.1.3.13. 1-(2,4-Difluorophenyl)-N′-[(Z)-(4-hydroxy-3-methoxyphenyl)methylidene]-4-methyl-5-[4-(trifluoromethyl) phenyl]-1H-pyrazole-3-carbohydrazide (**13**).* White solid in 86% yield; 245–246 °C. ^{1}H NMR (400 MHz, DMSO-d_6): δ 2.31 (s, 3H, CH_3), 3.84 (s, 3H, OCH_3), 6.84 (d, $J = 8$ Hz, 1H, ArH), 7.03 (dd, $J = 8.2$ and 2 Hz, 1H, ArH) 7.32–7.23 (m, 2H, ArH), 7.46–7.41 (m, 1H, ArH), 7.50 (d, $J = 8.0$ Hz, 2H, ArH), 7.79 (d, $J = 8.0$ Hz, 2H, ArH), 7.84–7.78 (m, 1H, ArH), 8.39 (s, 1H, NCH), 9.53 (s, 1H, ArOH), 11.64 (s, 1H, CONH). ^{13}C NMR (100 MHz, DMSO-d_6): δ 9.0, 55.5, 105.1 (dd, $J = 34.8$ and 23.8 Hz), 108.8, 112.5 (dd, $J = 18.6$ and 3.6 Hz), 115.4, 117.7, 122.2, 123.9 (q, $J = 270.8$ Hz), 123.5 (dd, $J = 12.2$ and 3.6 Hz),125.6, 125.9, 129.1 (q, $J = 32$ Hz), 130.2, 131.2 (d, $J = 10.6$ Hz), 132.5, 142.3, 144.3, 148.0, 148.3, 148.9, 156.3 (dd, $J = 251.6$ and 13.1 Hz), 158.1, 162.3 (dd, $J = 248.5$ and 11.4 Hz). FTIR (cm^{-1}): 3335.10, 3195.73, 3073.61, 2998.76, 1666.57, 1594.92, 1517.11, 1391.94, 1270.70, 1118.24. EI-MS m/z 530. (M+). HREI–MS = 530.1333 (calcd for $C_{26}H_{19}O_3N_4F_5$: 530.1372).

4.2. DPPH radical scavenging activity

DPPH radical scavenging activity was investigated according to the method of Sreejayan and Rao [41]. Briefly, 2.95 ml of ethanolic solution of 100 μM DPPH and 0.05 mL of samples at different concentrations were mixed. The control tube contains distilled water instead of sample. After incubation for 20 min at room temperature and in darkness the absorbance at 517 nm was recorded. The antioxidant capacity is given as percent (%) DPPH scavenging, calculated as [(optical density of control − optical density of sample)/(optical density of control) x 100].

4.3. ORAC assay

The assays were performed in a Synergy™ HT Multi-Mode Microplate Reader (BioTek Instruments, Inc., Winooski, VT, USA) and were based on the method described by Huang et al. [42]. In these assays 2,2′-Azobis(2-methylpropionamidine) dihydrochloride (AAPH), a water-soluble azo compound, was used as a peroxyl radical generator. Trolox, a water-soluble vitamin E analogue, was used as standard and fluorescein was used as fluorescent probe. Briefly, 25 μL of water, Trolox standards, diluted samples and diluted vehicle were mixed with 25 μL of 153 mM AAPH and with 150 μL of 50 nM fluorescein and incubated at 37 °C. The fluorescence was measured every min for a total of 90 min using fluorescence filters for an excitation wavelength of 485 nm and an emission wavelength of 520 nm. The ORAC values were calculated using the net area under the curves and were expressed as μmol of Trolox equivalents (TE) per gram of samples.

4.4. Animals

Male Wistar rats with 200–250 g of body weight were housed at standard laboratory conditions (22 ± 3 °C, 12 h day/night cycle), fed with a rodent pellet diet and water ad libitum. Animals described as 'fasted' were deprived of food for 16 h, but had free access to water. All animal procedures were conducted in accordance with Federal Regulations for Animal Experimentation and Care (NOM-062-ZOO-1999, SAGARPA, Mexico) and approved by the Institutional Animal Care and Use Committee based on the US National Institute for Health (publication No. 85-23, revised 1985).

4.5. Induction of diabetes

Diabetes was induced in overnight fasted rats by intraperitoneal (i.p.) injection of 110 mg/kg of nicotinamide 15 min before an i.p. injection of 65 mg/kg of streptozotocin dissolved in cold citrate buffer (pH 4.5). Rats with hyperglycemia (i.e. those with blood glucose between 200 and 350 mg/dL) were detected after 72 h using a glucometer and these were used for antidiabetic screening.

4.6. In vivo assay for antidiabetic activity

All compounds (50 mg/kg) were dissolved in Tween 80 at 10% in water (vehicle) and administered intragastrically to groups of five diabetic rats; control groups of vehicle (1 mL/rat) and glibenclamide (5 mg/kg) were also administered for negative control and drug reference. Blood samples were collected from the tail vein at 0, 3, 5 and 7 h after administration and glucose was measured using a commercial glucometer. The percentage of glycemia variation was calculated in relation to initial levels (0 h) using the formula: % variation of glycemia = [(Gx-G0)/G0] X 100, where G0 were the initial glycemia values and Gx were the glycemia values at T1, T3, T5 and T7 h, respectively. All values are expressed as mean ± S.E.M. the significance was estimated by an analysis of variance (ANOVA), $p < 0.05$ implies significance [43].

4.7. Computational details

All electronic calculations were performed with the Gaussian 09 package of programs [44] using a methodology previously reported [45,46]. For the identification of the most stable hydrazone isomer, geometry optimizations and frequency calculations of compounds **2** and **13** were carried out using the functional B3LYP and the 6-31G+(d) basis set, in conjunction with the PCM [47] continuum model using water as solvent. Since B3LYP has not be recommended for kinetic studies, we employed an M06-2X [34] and the 6–31++G(d,p) basis set, in conjunction with the SMD continuum model using water as solvent [48] to carried out geometry optimizations and frequency calculations. This methodology has been previously used in other kinetic studies with high accuracy and successfulness. Unrestricted calculations were used for open shell systems. Local minima and transition states were identified by the number of imaginary frequencies (0 and 1, respectively). Relative energies are calculated with respect to the sum of the isolated reactants. Thermodynamic corrections at 298.15 K were included in the calculation of relative energies, which correspond to 1 M standard state. In addition the solvent cage effects have been included according to the corrections proposed by Okuno [49], taking into account the free volume theory [50]. The expression used to correct the Gibbs free energy is:

$$\Delta G_{sol}^{FV} = \Delta G_{sol}^{0} - RT\left\{\ln\left[n10^{(2n-2)}\right] - (n-1)\right\} \quad (1)$$

where n represents the molecularity of the reaction. According to expression (1), the entropy loss in solution causes ΔG to decrease by 2.54 kcal mol^{-1} for bimolecular reactions, at 298.15 K. This correction is important because the cage effects of the solvent reduce the entropy loss associated with any chemical reaction whose molecularity is equal or larger than two.

The rate constants (k) were calculated using the Conventional

Transition State Theory (TST) [51–53]:

$$k = \sigma\kappa \frac{k_B T}{h} e^{\frac{-\Delta G^{\neq}}{RT}} \quad (2)$$

where k_B and h are the Boltzmann and Planck constants; $\Delta G^{\neq}$ is the Gibbs free energy of activation; σ represents the reaction path degeneracy, accounting for the number of equivalent reaction paths; and κ accounts for tunneling corrections. The latter, which are defined as the Boltzmann average of the ratio of the quantum and the classical probabilities, were calculated using the Zero Curvature Tunneling corrections (ZCT) [54].

Acknowledgments

Financial support from the Instituto de Ciencia y Tecnología del Distrito Federal (ICYTDF235/2010) is acknowledged. Eduardo Hernández-Vázquez is granted to the CONACyT for his fellowship (number 216082). We also thank to Rosa Isela del Villar, Georgina Duarte, Margarita Guzmán and Marisela Gutiérrez for the analytical support.

Appendix A. Supplementary data

Supplementary data related to this article can be found at http://dx.doi.org/10.1016/j.ejmech.2015.06.010.

References

[1] P. Rosen, P.P. Nawroth, G. King, W. Moller, H.J. Tritschler, L. Packerm, The role of oxidative stress in the onset and progression of diabetes and its complications: a summary of a Congress Series sponsored by UNESCOMCBN, the American Diabetes Association, and the German Diabetes Society, Diabetes Metab. Res. Rev. 17 (2001) 189–212.
[2] D. Pitocco, F. Zaccardi, E. Di Stasio, F. Romitelli, E. Santini, C. Zuppi, G. Ghirlanda, Oxidative stress, nitric oxide, and diabetes, Rev. Diabet. Stud. 7 (2010) 15–25.
[3] A.C. Maritim, R.A. Sanders, J.B. Watkins, Diabetes, oxidative stress, and antioxidants: a review, J. Biochem. Mol. Toxicol. 7 (2003) 24–38.
[4] A. Ceriello, Oxidative stress and glycemic regulation, Metabolism 49 (2000) 27–29.
[5] J.L. Evans, I.R. Goldfine, B.A. Maddux, G.M. Grodssky, Are oxidative stress-activated signaling pathways mediators of insulin resistance and β-cell dysfunction? Diabetes 52 (2003) 1–8.
[6] J.S. Johansen, A.K. Harris, D.J. Rychly, A. Ergul, Oxidative stress and the use of antioxidants in diabetes: linking basic science to clinical practice, Cardiovasc. Diabetol. 4 (2005) 5.
[7] L. Kiss, C. Szabó, The pathogenesis of diabetic complications: the role of DNA injury and poly(ADP-ribose) polymerase activation in peroxynitrite-mediated cytotoxicity, Mem. Inst. Oswaldo Cruz 100 (2005) 29–37.
[8] F. Giacco, M. Brownlee, Oxidative stress and diabetic complications, Circ. Res. 107 (2010) 1058–1070.
[9] J.L. Rains, S.K. Jain, Oxidative stress, insulin signaling, and diabetes, Free Radic. Biol. Med. 50 (2011) 567–575.
[10] P. Krishan, V.A. Chakkarwar, Diabetic nephropathy: aggressive involvement of oxidative stress, J. Pharm. Educ. Res. 2 (2011) 35–41.
[11] S.P. Wolff, Z.Y. Jiangm, J.V. Hunt, Protein glycation and oxidative stress in diabetes mellitus and ageing, Free Radic. Biol. Med. 10 (1991) 339–352.
[12] A. Bierhaus, S. Schiekofer, M. Schwaninger, M. Andrassy, P.M. Humpert, J. Chen, M. Hong, T. Luther, T. Henle, I. Kloting, M. Morcos, M. Hofmann, H. Tritschler, B. Weigle, M. Kasper, M. Smith, G. Perry, A.M. Schmidt, D.M. Stern, H.U. Haring, E. Schleicher, P.P. Nawroth, Diabetes-associated sustained activation of the transcription factor nuclear factor-κB, Diabetes 50 (2001) 2792–2808.
[13] M.R. Hayden, S.C. Tyagi, Islet redox stress: the manifold toxicities of insulin resistance, metabolic syndrome and amylin derived islet amyloid in type 2 diabetes mellitus, JOP 3 (2002) 86–108.
[14] N.F. Wiernsperger, Oxidative stress as a therapeutic target in diabetes: revisiting the controversy, Diabetes Metab. 29 (2003) 579–585.
[15] G. Baydas, H. Canatan, Comparative analysis of the protective effects of melatonin and vitamin E on streptozocin-induced diabetes mellitus, J. Pineal Res. 32 (2002) 225–230.
[16] L. Packer, K. Kraemer, G. Rimbach, Molecular aspects of lipoic acid in the prevention of diabetes complications, Nutrition 17 (2001) 888–895.
[17] D. Mekinova, V. Chorvathova, K. Volkovova, M. Staruchova, E. Grancicova, J. Klvanova, R. Ondreicka, Effect of intake of exogenous vitamins C, E and β-carotene on the antioxidative status in kidneys of rats with streptozotocin-induced diabetes, Nahrung 39 (1995) 257–261.
[18] A.D. Kloet, S.C. Woods, Endocannabinoids and their receptors as targets for obesity therapy, Endocrinology 150 (2009) 2531–2536.
[19] J. Tam, V.K. Verumi, J. Liu, S. Bátkau, B. Mukhopadhyay, G. Godlewsky, D. Osei-Hyiaman, S. Ohnuma, S.V. Ambudkar, J. Pickel, A. Makriyannis, G. Kunos, Peripheral CB1 cannabinoid receptor blockade improves cardiometabolic risk in mouse models of obesity, J. Clin. Invest. 120 (2010) 2953–2966.
[20] L. Bellocchio, C. Cervino, R. Pasquali, U. Pagotto, Cannabinoid type 1 receptor: another arrow in the adipocytes' bow, J. Neuroendocrinol. 20 (2008) 130–138.
[21] S. Engeli, Peripheral metabolic effects of endocannabinoids and cannabinoid receptor blockade, Obes. Facts 1 (2008) 8–15.
[22] E. Hernández-Vázquez, R. Aguayo-Ortiz, J.J. Ramírez-Espinosa, S. Estrada-Soto, F. Hernández-Luis, Synthesis, hupoglycemic activity and molecular modeling studies of pyrazole-3-carbohydrazides designed by a CoMFA model, Eur. J. Med. Chem. 69 (2013) 10–21.
[23] I. Seghrouchni, J. Drai, E. Bannier, J. Rivière, P. Calmard, I. Garcia, J. Orgiazzi, A. Revol, Oxidative stress parameters in type I, type II and insulin-treated type 2 diabetes mellitus; insulin treatment efficiency, Clin. Chim. Acta 321 (2002) 89–96.
[24] E. Anouar, C.A. Calliste, P. Kosinová, F. Di-Meo, J.L. Duroux, Y. Champavier, K. Marakchi, P. Trouillas, Free radical scavenging properties of guaiacol oligomers: a combined experimental and quantum study of the guaiacol-moiety role, J. Phys. Chem. A 113 (2009) 13881–13891.
[25] S.A. Ordoudi, M.Z. Tsimidou, A.P. Vafiadis, E.G. Bakalbassis, Structure-DPPH* scavenging activity relationships: parallel study of catechol and guaiacol acid derivatives, J. Agric. Food Chem. 54 (2006) 5763–5768.
[26] A. Sharma, S. Bhardwaj, A.S. Mann, S. Jain, M. Kharya, Screening methods of antioxidant activity: an overview, Pharmacogn. Rev. 1 (2007) 232–238.
[27] R.L. Prior, X. Wu, K. Schaich, Standardized methods for the determination of antioxidant capacity of phenolics in foods and dietary supplements, J. Agric. Food Chem. 53 (2005) 4290–4302.
[28] N.R. Perron, J.L. Brumaghim, A review of the antioxidant mechanisms of polyphenol compounds related to iron binding, Cell Biochem. Biophys. 53 (2009) 75–100.
[29] P. Molyneux, The use of the stable free radical diphenylpicrylhydrazyl (DPPH) for estimating antioxidant activity, J. Sci. Technol. 26 (2004) 211–219.
[30] M. Zulueta, M.J. Esteve, A. Frígola, ORAC and TEAC assays comparison to measure the antioxidant capacity of food products, Food Chem. 114 (2009) 310–316.
[31] R. Lan, Q. Liu, P. Fan, S. Lin, S.R. Fernando, D. McCallion, R. Pertwee, A. Makriyannis, Structure-activity relationships of pyrazole derivatives as cannabinoid receptor antagonists, J. Med. Chem. 42 (1999) 769–776.
[32] R.J. Chorvat, Pheripherally restricted CB1 receptor blockers, Bioorg. Med. Chem. Lett. 23 (2013) 4751–4760.
[33] G. Litwinienko, K.U. Ingold, Solvent effects on the rates and mechanisms of reaction of phenols with free radicals, Acc. Chem. Res. 40 (2007) 222–230.
[34] Y. Zhao, D.G. Truhlar, The M06 suite of density functionals for main group thermochemistry, thermochemical kinetics, noncovalent interactions, excited states, and transition elements: two new functionals and systematic testing of four M06-class functionals and 12 other functionals, Theor. Chem. Acc. 120 (2008) 215–241.
[35] A. Galano, J.R. León-Carmona, R. Álvarez-Idaboy, Influence of the environment on the protective effects of guaiacol derivatives against oxidative stress: mechanism, kinetics, and relative antioxidant activity, J. Phys. Chem. B 116 (2012) 7129–7137.
[36] N.V. Shorina, D.S. Kosyakov, K.G. Bogolitsyn, Acidity of guaiacol derivatives in water-acetone mixtures, Russ. J. Appl. Chem. 78 (2005) 125–129.
[37] G. Litwinienko, K.U. Ingold, Abnormal solvent effects on hydrogen atom abstractions. 1. the reactions of phenols with 2,2-diphenyl-1-picrylhydrazyl (dpph•) in alcohols, J. Org. Chem. 68 (2003) 3433–3438.
[38] G. Litwinienko, K.U. Ingold, Abnormal solvent effects on hydrogen atom abstraction. 2. Resolution of the curcumin antioxidant controversy. The role of sequential proton loss electron transfer, J. Org. Chem. 69 (2004) 5888–5896.
[39] G. Litwinienko, K.U. Ingold, Abnormal solvent effects on hydrogen atom abstraction. 3. Novel kinetics in sequential proton loss electron transfer chemistry, J. Org. Chem. 70 (2005) 8982–8990.
[40] G. Litwinienko, U.K. Ingold, Solvent effects on the rates and mechanisms of reaction of phenols with free radicals, Acc. Chem. Res. 40 (2007) 222–230.
[41] N. Sreejayan, M.N. Rao, Free radical scavenging activity of curcuminoids, Arzneimittelforschung 46 (1996) 169–171.
[42] D. Huang, B. Ou, M. Hampsch-Woodill, J. Flanagan, R. Prior, High-throughput assay of oxygen radical absorbance capacity (ORAC) using a multichannel liquid handling system coupled with a microplate fluorescence reader in 96-well format, J. Agric. Food Chem. 50 (2002) 4437–4444.
[43] J.J. Ramírez-Espinosa, M.Y. Rios, S. López-Martínez, F. López-Vallejo, J.L. Medina-Franco, P. Paoli, G. Camici, G. Navarrete-Vázquez, R. Ortiz-Andrade, S. Estrada-Soto, Antidiabetic activity of some pentacyclic acid triterpenoids, role of PTP-1B: in vitro, in silico, and in vivo approaches, Eur. J. Med. Chem. 46 (2011) 2243–2251.
[44] M.J. Frisch, G.W. Trucks, H.B. Schlegel, G.E. Scuseria, M.A. Robb, J.R. Cheeseman, G. Scalmani, V. Barone, B. Mennucci, G.A. Petersson, et al., Gaussian 09, Revision B.01, Gaussian, Inc., Wallingford CT, 2009.
[45] A. Galano, R. Alvarez-Idaboy, A computational methodology for accurate

predictions of rate constants in solution: application to the assessment of primary antioxidant activity, J. Comput. Chem. 34 (2013) 2430–2445.
[46] A. Galano, R. Alvarez-Idaboy, Kinetics of radical-molecule reactions in aqueous solution: a benchmark study of the performance of density functional methods, J. Comput. Chem. 35 (2014) 2019–2026.
[47] S. Miertus, J. Tomasi, Approximate evaluations of the electrostatic free energy and internal energy changes in solution processes, Chem. Phys. 65 (1982) 239–241.
[48] A.V. Marenich, C.J. Cramer, D.G. Truhlar, Universal solvation model based on solute electron density and on a continuum model of the solvent defined by the bulk dielectric constant and atomic surface tensions, J. Phys. Chem. B 113 (2009) 6378–6396.
[49] Y. Okuno, Theoretical investigation of the mechanism of the Baeyer-Villiger reaction in nonpolar solvents, Chem. Eur. J. 3 (1997) 210–218.
[50] S.W. Benson, in: The Foundations of Chemical Kinetics, McGraw-Hill, New York, 1960, pp. 504–508 (Chapter XV).
[51] H. Eyring, The activated complex in chemical reactions, J. Chem. Phys. 3 (1935) 107–115.
[52] M.G. Evans, M. Polanyi, Some applications of the transition state method to the calculation of reaction velocities, especially in solution, Trans. Faraday Soc. 31 (1935) 875–894.
[53] D.G. Truhlar, W.L. Hase, J.T. Hynes, Current status of transition-state theory, J. Phys. Chem. 87 (1983) 2664–2682.
[54] D.G. Truhlar, A. Kuppermann, Exact tunneling calculations, J. Am. Chem. Soc. 93 (1971) 1840–1851.